Developments in the Built Environment 18 (2024) 100456

Contents lists available at ScienceDirect

Developments in the Built Environment

journal homepage: www.sciencedirect.com/journal/developments-in-the-built-environment

Effect of crystalline admixtures on shrinkage and alkali-silica reaction of biochar-cementitious composites

Xuqun Lin [a], Arnaud Castel [a], Zhizhong Deng [a], Biqin Dong [c], Xuanrui Zhang [a], Shishun Zhang [d], Wengui Li [b,*]

[a] School of Civil and Environmental Engineering, University of Technology Sydney, NSW, 2007, Australia
[b] Centre for Infrastructure Engineering and Safety, School of Civil and Environmental Engineering, The University of New South Wales, NSW, 2052, Australia
[c] College of Civil and Transportation Engineering, Guangdong Provincial Key Laboratory of Durability for Marine Civil Engineering, Shenzhen University, Guangdong, 518060, China
[d] School of Civil and Hydraulic Engineering, Huazhong University of Science and Technology, Wuhan, 430074, China

ARTICLE INFO

Keywords:
Self-healing
Crystalline admixture
Biochar
Shrinkage
Alkali-silica reaction

ABSTRACT

This study investigated effects of crystalline admixture (CA) on shrinkage and alkali-silica reaction behaviours of biochar-cementitious composites. Addition of 1–1.5 wt% superabsorbent polymer (SAP) completely mitigated autogenous shrinkage while slightly increasing the 120-day total shrinkage of the SP-cement composite by 5.7%, resulting in the highest apparent porosity. 1–1.5 wt% CA addition did not affect autogenous shrinkage while slightly reducing the 120-day total shrinkage by 10.1%. The combination of CA and waste wood biochar (WWB) reduced autogenous shrinkage by 24.23% and 120-day total shrinkage by 23.6%, resulting in the lowest apparent porosity. The formation of hydration products in the WWB pores and on WWB surface densified the cementitious matrix, leading to a reduction in water evaporation. Furthermore, for specimens exposed to 1 M NaOH solution at 80 °C, CA addition significantly reduced the 120-day expansion by 50.6%, while the combination of CA and WWB addition reduced the 120-day expansion by 42.9%.

1. Introduction

Durable design is required to satisfy the requirements in numerous structural design codes, improving the structural resilience and durability of reinforced concrete structures (Amjad et al., 2023). Due to the brittle nature of the cementitious matrix, concrete structures suffer from a high risk of cracking as a result of service loading, restrained shrinkage, temperature fluctuation, or environmental deterioration (Cappellesso et al., 2023a; Zeinali et al., 2023). Crack initiation poses a significant challenge as aggressive ions would penetrate and damage the internal cementitious matrix, lowering the serviceability and durability of concrete structures (Cappellesso et al., 2023b; Liu et al., 2022). Typically, due to the ingress of harmful substances, such as chlorides, corrosion products would form at the steel rebar-cementitious matrix interface, reducing the bearing capacity of the structures (Hermawan et al., 2023; Macdonald et al., 2021). Repairing cracked concrete leads to substantial financial costs. Several studies (Cassidy et al., 2015; Mohammed et al., 2020) mentioned that repairing and maintenance costs are approximately $13 billion annually due to corrosion-related structural damages and cracks in Australia. Hence, appropriately preventive techniques for controlling undesirable concrete cracking or corrosion damages are highly required.

Many studies (Mohammed et al., 2020; Xiao et al., 2023; De Souza and Sanchez, 2023) stated that self-healing concrete was considered as a promising method in timely sealing cracks, requiring no additional labour and maintenance costs. Tittelboom and Belie (Van Tittelboom and De Belie, 2013) reported that there were two main self-healing process, including autonomous and autogenous self-healing. For autonomous self-healing process, many studies utilised capsule-filling self-healing agents, including vascular networks (Wan et al., 2023a, 2023b; De Nardi et al., 2023) or sporulated-form bacterial (Cappellesso et al., 2023a; Xiao et al., 2023; Akhtar et al., 2023). According to Cappellesso et al. (2023a), the main healing mechanism of bacterial-based agents was that when capsules were broken during cracking, the bacterial with metabolic activities would promote calcite precipitation to seal the cracked region, requiring moisture, nutrient for calcium ions, and oxygen.

* Corresponding author. Centre for Infrastructure Engineering and Safety, School of Civil and Environmental Engineering, The University of New South Wales, NSW, 2052, Australia.
E-mail address: wengui.li@unsw.edu.au (W. Li).

https://doi.org/10.1016/j.dibe.2024.100456
Received 18 February 2024; Received in revised form 6 May 2024; Accepted 8 May 2024
Available online 12 May 2024

Several studies (Su et al., 2021; Wu et al., 2020) highlighted that it was necessary to provide a protective treatment for microbial agents, ensuring the survival of bacteria during casting and hydration. However, Wu et al. (2020) pointed out that by adding 1–4 wt% microcapsules, the compressive strength of the bacterial-cement composites was reduced by 15–34%. They described that the application of microcapsules affected the workability of the cementitious composites. Meanwhile, glass-based capsulation may be damaged to release healing agents before cracking (Wan et al., 2023a), affecting the overall self-healing efficiency. In contrast to the autonomous self-healing, many researchers (Tian et al., 2022; Chindasiriphan et al., 2020; Zhang et al., 2021; Xue et al., 2021) defined autogenous healing as the healing process by continuous hydration of unhydrated products or calcite precipitation sealing the cracks. Although crystalline admixtures (CAs) are normally used as permeability-reducing agents (Hu et al., 2022; de Souza Oliveira et al., 2021), several studies (Zhang et al., 2021; Xue et al., 2020, 2021; Li et al., 2020a; Wang et al., 2023) used CAs as autogenous healing agent sealing cracks in the cementitious matrix. Wang et al. (2018) suggested that CA not only promoted a denser cementitious microstructure by inducing pore-blocking crystalline deposits to reduce both porosity and permeability but also improved the self-healing efficiency of the CA-cement composites.

Since CA contains 60–80 wt% cement powder (Penetron, 2023), CA addition does not negatively affect the workability (Wang et al., 2018; Munn et al., 2003) and setting time (Zheng et al., 2019) of the cementitious composites, highlighting the favourable benefit in terms of practicality when compared with the application of bacterial-based capsulation. Borg et al. (2018) investigated the compressive strength of mortar specimens with 1 wt% CA, and they found that CA addition promoted 12.6% increment of compressive strength when compared to a reference group. Many studies (FloresM et al., 2015; Chandra and Ravitheja, 2019) agreed that the main reason for strength improvement was that CA promoted the formation of calcite and C–S–H gels filling pores and voids in the cementitious matrix, improving matrix compactness to resist higher loads. However, Oliveira et al. (de Souza Oliveira et al., 2021) revealed that although CA promoted a denser microstructure in the CA-cement matrix, there was limited improvement on tensile strength, due to the brittle nature of the cementitious matrix. Likewise, Sisomphon et al. (2013) observed that there was a slight strength improvement of approximately 4.8% on the flexural capacity after adding 1.5 wt% CA. Oliveira et al. (de Souza Oliveira et al., 2021) reported that another benefit of CA-induced denser microstructure was that it also promoted structural resilience, protecting internal steel rebars. Meanwhile, many studies (Li et al., 2020a; Azarsa et al., 2019) highlighted that CA stimulated crystalline deposits in filling pores in the cementitious matrix, reducing capillary channels to resist aggressive-ion penetration. Zhang et al. (2021) reported that CA addition not only reduced the permeability of the CA-cement composites, but also improved the closure rate of cracked samples. Lauch et al. (2022a) added 2 wt% CA in the cementitious composites, and they found that cracked samples were fully sealed when exposed to wet/dry cycles. Xue et al. (2021) cured pre-cracked CA-cement samples in water and NaCl solutions. They concluded that due to the additional formation of Friedel's salt (Fs), specimens cured in NaCl solution had faster crack closure when compared with samples cured in water. Furthermore, Guenca et al. (Cuenca et al., 2021) observed that CA offered continuous healing capacity in a multi-cracking experiment. They found that the reopening crack due to the second cracking area was healed up to 70%. Several studies (Lucas et al., 2016; Guan et al., 2020) explained that due to the accumulation of the special chemicals in CA, being the main stimulator of self-healing products, reopening crack would be sealed in the presence of moisture. Although the effects of CA on the mechanical properties and self-healing efficiency of cementitious composites are well documented and investigated, there are limited evidence showing the potential effects of CA on the volume stability and durability properties of CA-cement composites, such as shrinkage deformation and alkali-silica reactions (ASRs). Regarding ASRs, the potential effects of CA addition on the ASR behaviours of the CA-cement composites are not well understood. As a result, the application of the CA addition on the cementitious composites may be affected due to its potential to deteriorate ASRs (Dong et al., 2021; Dong et al., 2022; Xue et al., 2019; Xue et al., 2020).

Based on the findings by Lin et al. (2023), biochar was a proper alternative to partially replace cement, improving mechanical strengths and durability properties of the biochar-cement composites. Javed et al. (2022) found that using 2 wt% bagasse biochar in replacing cement led to a strength increase of 18% on the compressive strength of the biochar-cement composite when compared to the reference group. Several studies (Xu and Wang, 2021; Wang et al., 2019a) observed that the presence of biochar promoted the cement hydration and filled in pores and voids, leading to a denser microstructure to reduce chloride diffusion. Similarly, Gupta et al. (2018) found that using biochar to partially replace cement reduced the permeability of the cementitious composites. As a results, more studies are required to investigate the feasibility of recycling different biomass wastes to produce biochar in Australia, reducing the cost and resources in managing these wastes by burning or landfill. This study considers using local biochar to partially replace a portion of the cement to investigate the volume stability properties of the biochar-cement composites, aiming to provide more results in understanding how biochar may affect the properties of the cementitious composites.

In this study, the potential effects of CA addition on shrinkage and ASRs were investigated. The investigations of shrinkage and ASRs complied with AS 2350.13 (AS 2350, 2006) and AS 1141.60.1 (AS 1141, 2014) respectively. Both tests were performed for 120-day curing to understand how CA addition would affect the volume stability and durability properties of the CA-cement composites. Apparent porosity analysis was carried out to determine differences between the porosity of samples, and Scanned electron microscopy (SEM) was used to investigate the interfacial-transition zones (ITZs) between reactive aggregates and the cementitious matrix in ASRs experiment. In addition, biochar was used in this study to assess its potential to improve the properties of the cementitious matrix. Furthermore, the analysis of raw materials included SEM image, X-ray fluorescence spectrometry (XRF), and particle size distribution (PSD) were carried out.

2. Experimental program

2.1. Raw materials

General purpose (GP) cement produced by Boral Australia, was utilised as the major binder in this study. Commercially available superabsorbent polymers (SAP), namely DESAP® by Global Spill Control (Australia), was used as one of the healing agents in this study. According to Lauch et al. (2022b), SAP was the polymers formed by cross-linked polyacrylamide in powder form. Based on several studies (Li et al., 2020b; Aghaee and Khayat, 2022), SAP could properly mitigate the autogenous shrinkage of SAP-cement composites. Similarly, commercially available crystalline admixtures (CA), traded by PENETRON Admix® (Australia), was selected as another healing agent for investigations relating to both shrinkage and alkali-silica reactions. CA consists of a large amount of CaO, a certain amount of silica, and several patent-protected chemicals. Blended waste wood biochar was a commercial product, obtained from Green Man Char (Australia), which was produced from oxygen-limited pyrolysis based on locally constructional waste wood. Fig. 1 illustrates the images of the different raw materials. Originally blended biochar was ground into fine powder, namely WWB. The particle size distribution (PSD) of CA and WWB was analysed by Malvern 2000 Particle Size Analyser. As depicted in Fig. 2, the maximum particle size of WWB particle is 200 μm, providing proper filler effect in blocking voids in the cementitious matrix. Due to its large cement content (60–80%), the PSD of CA is very similar to that of GP cement.

Fig. 1. Morphology of raw materials: (a) PENETRON CA, (b) SAP, (c) Original blended biochar, and (d) WWB.

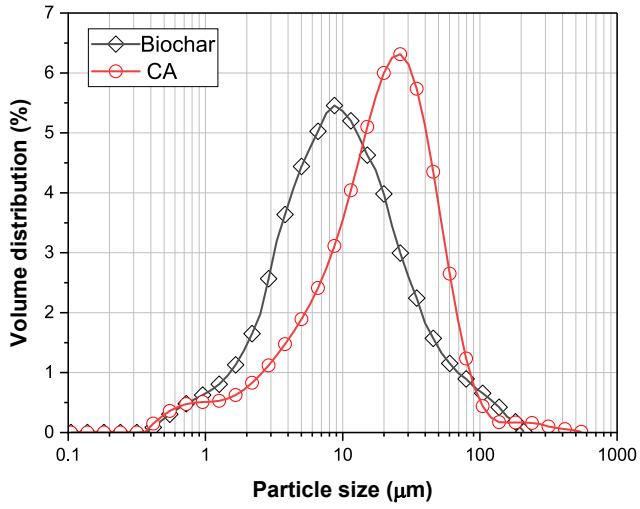

Fig. 2. Particle size distribution of CA and WWB.

However, since CA contains several special chemical powders, particles being larger than 100 μm and up to 500 μm were identified.

Fig. 3(a) and (b) present the micro-morphology of CA and WWB respectively. CA contains many irregular-shaped particles, and Fig. 3(b) reveals that WWB microstructure is porous with thick wall. Guizani et al. (2017) reported that although beech wood biochar (BWB) was processed by 500–600 °C pyrolysis, a thin wall was observed in the microstructure of BWB particles, highlighting the variability of the biochar microstructure. As illustrated in Fig. 3(b), the shapes of macro-pores in WWB are randomly formed and distributed, and there is structural disintegration at the edge of WWB particle during the grinding process by ball milling. Overall, the macro-pores of WWB are oval shape ranging from to 1 μm 5 μm. XRF results in Table 1 show the chemical compositions of the three different raw materials. Although CA contains up to 80% cement, General purpose cement (Boral, Australia) has higher contents of calcium oxide (CaO), silica (SiO_2), and aluminium oxide (Al_2O_3) than CA (PENETRON, Australia). However, it should be noted that CA has higher contents of sodium oxide (Na_2O) and magnesium oxide (MgO), being 9.15% and 3.27% respectively. One interpretation could be that CA may contain various sodium-based chemicals to promote self-healing. The XRF results reveal that the SiO_2/CaO ratio of WWB is 2.95, significantly higher than that (SiO_2/CaO ratio = 0.3) of cement. If the content of amorphous silica being exposed to WWB surface is relatively higher, it could improve the pozzolanic reaction during the hydration process.

2.2. Sample preparation

This study aimed to investigate the impact of different healing agents on the resistance to shrinkage and the potential effect of CA addition on resisting alkali-silica reactions, as shown in Fig. 4. As a result, different prism moulds were utilised, including shrinkage mould (40 mm × 40 mm × 160 mm) and AMBT mould (25 mm × 25 mm × 25 mm). Lin et al. (2023) suggested that 2 wt% biochar was the optimal percentage to replace cement, providing a favourable reduction in shrinkage. Hence, 2 wt% WWB was utilised in replacing GP cement to cast biochar-cementitious composites. Due to the addition of SAP, an extra amount of water was essential to maintain the effective water-to-cement

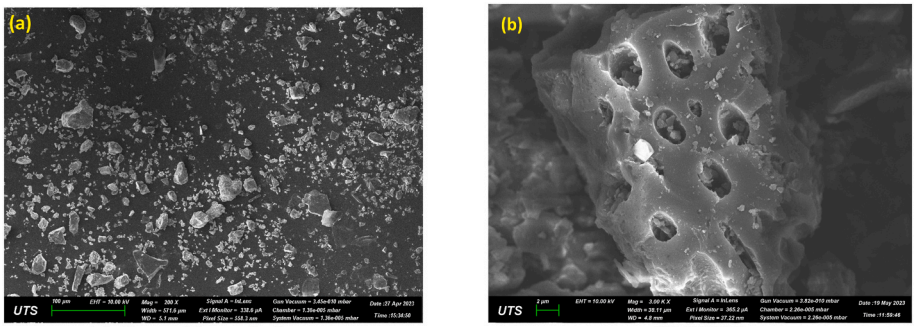

(a) Crystalline admixture (b) WWB

Fig. 3. Morphologies of Ca and WWB.

Table 1
Chemical compositions of raw materials.

Chemical compositions (%)	CA	General Purpose Cement	WWB
CaO	49.24	63.73	19.73
Al_2O_3	3.73	5.14	3.95
SiO_2	14.15	18.94	58.20
P_2O_5	0.17	0.20	2.29
SO_3	1.83	2.49	1.35
K_2O	0.74	0.47	2.88
TiO_2	0.12	0.29	0.27
V_2O_5	<0.01	0.02	<0.01
Cr_2O_3	0.01	0.02	0.05
Mn_3O_4	0.08	0.19	0.50
Fe_2O_3	1.76	3.00	1.67
Na_2O	9.15	0.25	5.10
MgO	3.27	1.48	3.45
LOI	15.78	4.09	0.50

ratio of 0.35. This study adopted the methodology by Wang et al. (2022a). They conducted a trial-and-error test to find the optimal volume of extra water for the samples with SAP. Aiming to maintain a comparable workability, the required amount of additional water and mixture details for prisms were in Table 2. Similarly, due to the addition of WWB, a trial-and-error test was performed to determine the optimal dosage of superplasticiser to keep a comparable slump. Meanwhile, for the accelerated mortar bar test (AMBT), dacite fine aggregates (reactive sand) were crushed from dacite coarse aggregates and a commercial product of sodium hydroxide pellets (Rowe Scientific, Australia) was selected to prepare the 1 M NaOH solution.

Initially, all materials were pre-mixed for 3 min using a 5-L Hobart mixer to obtain a proper powder mixture. Then, 1/3 volume of water was added in the mixer for another l-minute of low-speed mixing. After that, the rest of water was added with medium-speed mixing for 3 min. Then, cementitious mixture on the bowl's wall was shovelled to avoid loss of binder materials, and mixing was continued for 1 min. Fresh cement paste for shrinkage test and fresh cement mortar for AMBT was then poured into the corresponding moulds and were vibrated for 3 min

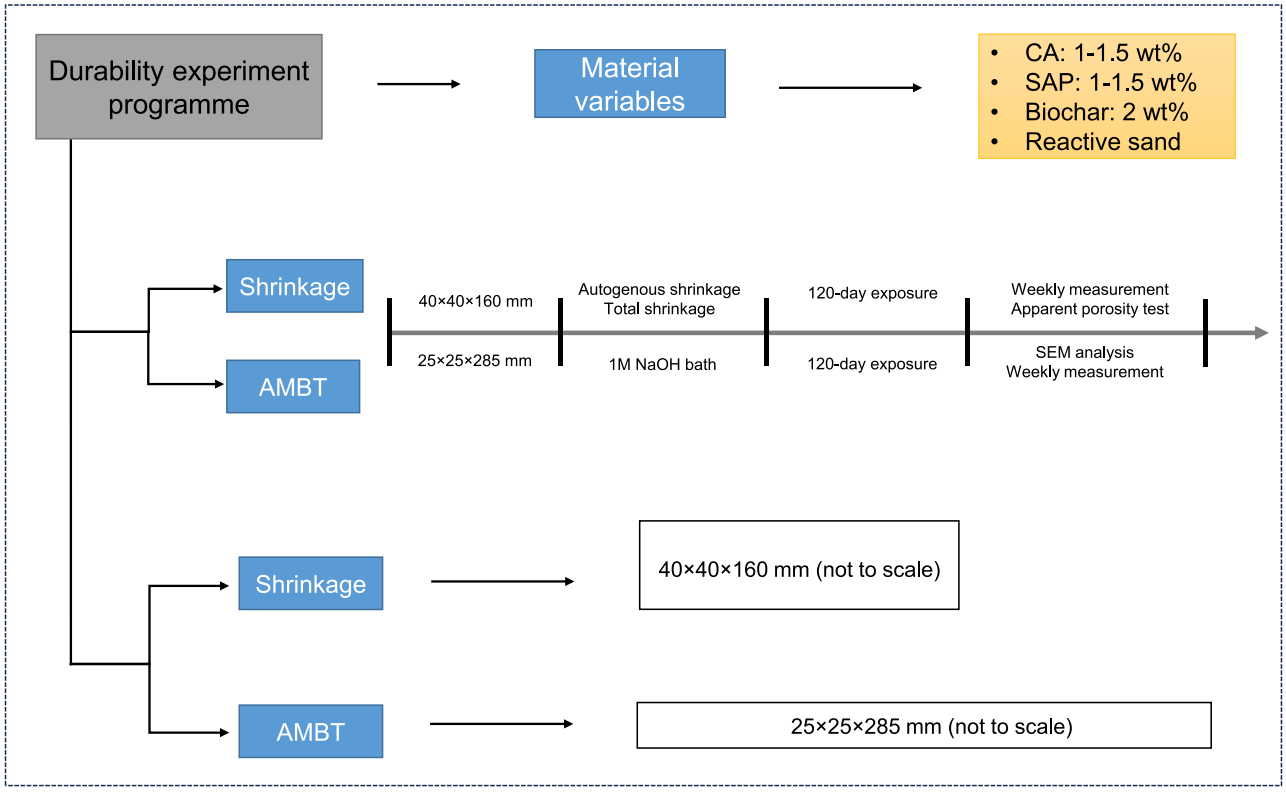

Fig. 4. Experimental program.

Table 2
Mix design of shrinkage and AMBT tests.

Tests	Samples	GPC	Reactive sand	Water	CA	SAP	WWB	Extra water	Superplasticizer	Slump (mm)
Shrinkage	CO	1	–	0.35	–	–	–	–	–	231 ± 1.3
	CA	1	–	0.35	0.01	–	–	–	–	229 ± 2.5
	CA15	1	–	0.35	0.015	–	–	–	–	228 ± 2.2
	SAP	1	–	0.35	–	0.01	–	0.11	–	229 ± 2.4
	SAP15	1	–	0.35	–	0.015	–	0.16	–	227 ± 1.2
	CB	0.98	–	0.35	0.01	–	0.02	–	0.008	228 ± 3.3
Accelerated mortar bar test	CO	1	2	0.35	–	–	0	–	–	210 ± 2.4
	CA	1	2	0.35	0.01	–	0	–	–	209 ± 3.1
	CB	0.98	2	0.35	0.01	–	0.02	–	0.008	211 ± 2.1

to remove air bubbles for uniform compaction. In this study, since three samples were created for each test, the same mixing process was repeated to produce sufficient paste and mortars samples for each test. Importantly, plastic foil was applied to cover all prism moulds till 24-h demoulding.

2.3. Experimental programme

2.3.1. Shrinkage

The shrinkage experiments were carried out to investigate both total shrinkage in Fig. 5(a) and autogenous shrinkage in Fig. 5(b) complying with AS 2350.13 (AS 2350, 2006), being the Australian Standard for investigating shrinkage of cement mortars. After demoulding, the samples length was measured using a digital comparator with an accuracy of ±0.001 mm, and all readings were repeated three times to appropriately record the initial length. Cementitious specimens for autogenous shrinkage measurements were covered with aluminium foil and sealed immediately in a plastic bag after the first measurement to avoid water evaporation. According to AS 2350.13 (Methods of testing portland, blended and masonry cements, Method 13: Determination of drying shrinkage of cement mortars) (AS 2350, 2006), all shrinkage specimens were then properly placed in a conditioned room with 50 ± 5% relative humidity and 23 ± 2 °C. During the length measurements, it should be noted that no moist curing was applied for all samples after demoulding.

The measurements were performed once a day for the first week, and then all specimen's length was measured weekly up to 120-day curing. Autogenous shrinkage and total shrinkage results were directly measured by the digital comparator. It should be noted that three samples were cast for each case, and the average values were used to plot the shrinkage results.

2.3.2. Accelerated mortar bar test

All AMBT specimens in Fig. 5(c) were demoulded after 24-h curing in the humidity cabinet, and initial lengths were measured. A 153-L autoclave (Zirbus LVSA 50/70) was utilised as the main heating station in this study. A temperature of 80 °C could be obtained within a few mins and the pressure remained as atmospheric pressure. According to AS 1141.60.1 (Methods for sampling and testing aggregates, Method 60.1: Potential alkali-silica reactivity - Accelerated mortar bar method) (AS 1141, 2014), AMBT samples should be placed in a container with 1 M NaOH solution. The container was immersed in the 80 °C water bath in the autoclave to accelerate ASR expansion. Similar to shrinkage measurements, all samples were measured once a day for the first week and measured once per week up to 120-day in the NaOH solution.

2.3.3. Apparent porosity analysis

Several studies (De Souza and Sanchez, 2023; Ahmadi Moghadam et al., 2020) suggested that the apparent porosity test could be used to investigate the pore volume differences of the cementitious matrix. This study adopted Archimedes method to analysis the apparent porosity of the total shrinkage specimens at 28-day exposure and 120-day exposure. It should be noted that additional three prisms were casted for 28-day apparent porosity test for each mix design. However, the 120-day apparent porosity test was measured using the total shrinkage

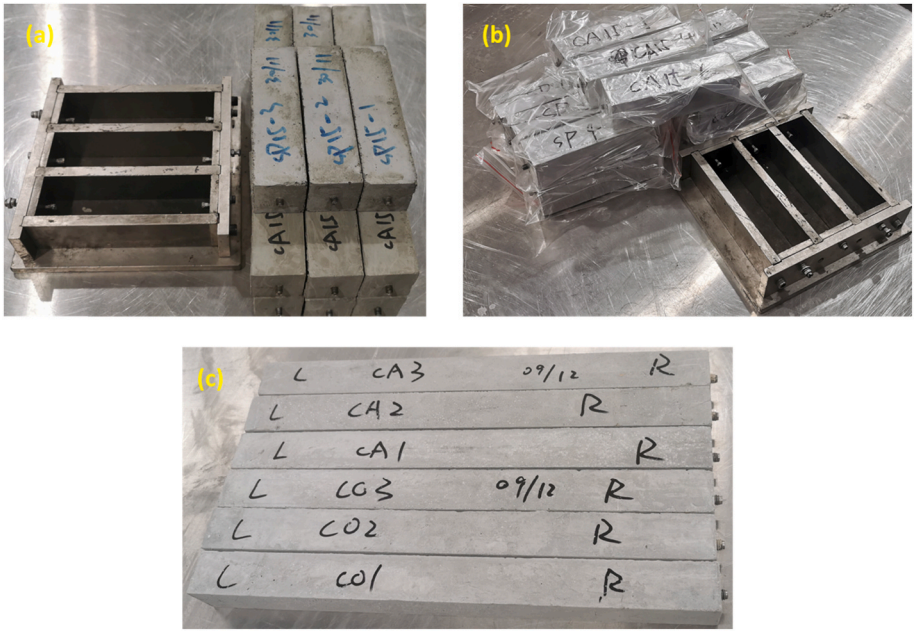

Fig. 5. Tests of cementitious composites: (a) total shrinkage test, (b) autogenous shrinkage test, and (c) AMBT test.

samples. Initially, the samples were fully immersed in distilled water for 48 h to a constant saturated mass before exposed to 105 °C, protecting pores structure in the high-temperature environment. Next, the samples were placed in the oven with 105 °C for 2 days to get a constant dry mass (m_d). Then the dried samples were placed in distilled water for another 48 h. After that, the submerged weight of the prisms was measured as (m_i), and the saturated weight (m_s) was measured by quickly wiping the surface water of the samples. Hence, the apparent porosity (P) was obtained by the following equation:

$$P = \frac{m_s - m_d}{m_s - m_i} \times 100\% \quad (1)$$

2.3.4. Microstructural analysis

High-resolution SEM equipment (Zeiss Supra 55VP) was used to analyse the microstructure of the shrinkage and AMBT samples. Before the SEM analysis, samples were crushed and dried in a vacuum oven at 50 °C for 3 days. Then, all samples were coated with gold by a coating machine (Leica EM ACE600 coater). After that, SEM analysis was performed by using a voltage of 10 kV. Meanwhile, aiming to classify the hydration products in a particular location, point scan of energy dispersive X-ray spectroscopy (EDS) in Zeiss Supra 55VP was utilised. It should be noted that 10 points were examined in each location to get an average result of Ca/Si ratio of the hydration products.

3. Experimental results

3.1. Autogenous shrinkage

Fig. 6 presents the autogenous shrinkage deformation of the samples with CA, SAP, and WWB. The addition of CA leads to a negligible reduction in autogenous shrinkage deformation. In Fig. 6, the autogenous shrinkage results of CA (black line) and CA15 (red line) are very similar to the reference group CO (blue line). The shrinkage deformation rate is gradually reduced, and a noticeable trend is that after 80-day exposure, the autogenous shrinkage values tend to remain stable. As aforementioned, each specimen was covered with aluminium foil and sealed in an individual plastic bag during 120-day testing period, preventing the moisture evaporation. Several studies (Aghaee et al., 2023; De Meyst et al., 2021) pointed out that internal curing due to water retention was an effective way in reducing the autogenous shrinkage of the cementitious composites. Due to the large amount of cement (up to 80%) in CA, CA does not affect the workability of the fresh cementitious paste by water retention, evidenced by the slump obtained with and without CA, being 229 ± 2.5 and 231 ± 1.3 respectively in Table 2.

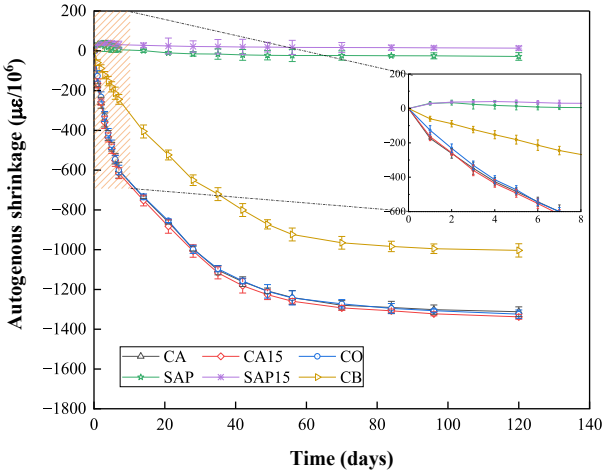

Fig. 6. Autogenous shrinkage results.

Likewise, Wang et al. (2018) also suggested that CA addition did not reduce the workability of the cementitious composites. Although addition of CA promotes a denser cementitious microstructure (Xue et al., 2021; Wang et al., 2018; FloresM et al., 2015; Chandra and Ravitheja, 2019), no water retention process is involved in the CA-cementitious composites for internal curing. As a result, 1–1.5 wt% CA addition does not lead to any reduction in the autogenous shrinkage deformation in Fig. 6. Hence, CA is not a proper cementitious supplementary material (CSM) allowing reduction in the autogenous shrinkage of the cementitious composites.

However, SAP addition dramatically reduces the autogenous shrinkage of the SAP-cementitious composites, being in good agreement with many studies (Rostami et al., 2021; Tu et al., 2019). As depicted in Fig. 6, instead of directly experiencing the autogenous shrinkage, the cement pastes with SAP expand during the early curing age (0–3 days). According to Snoeck et al. (2015), SAP particles can maintain the water retention process, resulting in an overall expansion of the SAP mixtures during the initial hydration stage. SAP15 samples show larger expansion than SAP group, and the shrinkage deformation of both SAP and SAP15 mixtures tend to remain stable after 7-day exposure. As a result, almost no autogenous shrinkage deformations are measured on the SAP-cementitious composites. Several studies (Aghaee et al., 2023; Snoeck et al., 2015) revealed that SAP particles gradually released retained water to reduce hydrostatic tension forces, preventing the autogenous shrinkage. It should be noted that, for SAP group, there is a small autogenous shrinkage deformation after 3-day exposure. This can be due to the end of the continuous SAP particle expansion, but the autogenous shrinkage remained flat after 7-day exposure. However, the actual effect of SAP on the autogenous shrinkage of the cementitious matrix highly depends on the water-releasing behaviours of SAP (Snoeck et al., 2015; Moelich et al., 2022). Unlike comparable elimination of the autogenous shrinkage by SAP observed in this study, Snoeck et al. (2015) observed that one of the SAP addition did not mitigate the autogenous shrinkage deformation. They stated that it was due to the relatively slow release or partially releasing of water content retained by SAP particles. In this study, the addition of 1–1.5 wt% SAP could almost eliminate autogenous shrinkage, and the higher dosage of SAP was the most effective.

Adding 2 wt% WWB to replace General purpose cement in the CA group, CB group led to an autogenous shrinkage deformations reduction of approximately 24.23% at 120-day exposure, compared to that of the reference group. Instead of sharply shrinking during the early curing period up to 7 days, the cementitious pastes with WWB experienced relatively slow shrinkage, reducing by approximately 59.19% shrinkage deformation at 7-day exposure. Similar findings were reported by several studies (Mo et al., 2019; Gupta et al., 2020). Gupta et al. (Gupta and Kua, 2019) suggested that due to water retention of pulverised biochar, relatively low w/c ratio (water/cement ratio) reduced the capillary porosity near the interfacial transition zones (ITZs). Meanwhile, biochar particles gradually release absorbed water, promoting additionally internal curing (Kua and Tan, 2023; Gupta and Kua, 2018). As a result, the self-desiccation of CB group is reduced due to both capillary porosity refinement and internal curing. Mo et al. (2019) observed approximately 19% shrinkage reduction at 7-day exposure, being significantly lower than this study. The first reason is that relatively larger pulverised biochar was used by Mo et al. (2019), while Lin et al. (2023) found that finer-size biochar particles could be more effective in reducing the shrinkage of the biochar-cementitious composites. Secondly, It should be noted that Mo et al. (2019) did not add superplasticiser to keep a comparable w/c ratio for the biochar-cementitious pastes, leading to improper biochar distribution. However, 0.8 wt% superplasticiser is added to improve the workability of the biochar-cement composites in this study, improving biochar distribution for porosity refinement. Overall, WWB could be considered as an appropriate alternative to replace cementitious binder in reducing the autogenous shrinkage of sustainable concrete.

3.2. Total shrinkage

Fig. 7 depicts the total shrinkage deformations of the cementitious pastes up to 120-day exposure. Several studies (Gupta et al., 2020; Wongkeo et al., 2012) suggested that capillary pore structure and refinement could be considered as the key factors affecting the evaporation rate of moisture in the cementitious matrix. In Fig. 7, the addition of CA and WWB significantly reduced the total shrinkage strain, and the addition of SAP only reduced the total shrinkage up to 4-day curing, but slightly increased the total shrinkage of the SAP-cement composites during at long term.

Considering the potential effect of CA addition on total shrinkage, CA and CA15 group show similar total shrinkage deformation subjected to 120-day exposure with negligible differences. When compared to the control group (blue line) in Figs. 7 and 13.4% and 10.9% shrinkage reduction is observed for CA (black line) and CA15 (red line) groups respectively at 7-day exposure. Many studies (FloresM et al., 2015; Wang et al., 2019b) observed that CA promoted pore-blocking crystals, improving the compactness of the CA-cement matrix. As a result, a denser microstructure would reduce the evaporation rate of moisture in both CA and CA15 group, leading to a reduction in the total shrinkage strains. However, CA addition does not affect the trend of the shrinkage deformation when compared to that of the control group. The reason could be that although CA refines the microstructure of the cementitious matrix at the early age (up to around 28 days), there is no major change in the inherent cementitious nature at the longer age due to the loss of water. Thus, there are only slight changes in the trend of total shrinkage when compared to the reference group CO. 1 wt% CA addition leads to 8.4% and 10.1% reduction in 28-day and 120-day shrinkage strains respectively, while 1.5 wt% CA addition promotes 7.1% and 9.2% reduction on 28-day and 120-day shrinkage strains respectively. Although CA promotes a denser cementitious microstructure, the reduction rate of total shrinkage does not increase when exposing to longer-term curing. Hu et al. (2022) stated that the presence of moisture was the crucial factor in activating the special chemicals in CA to stimulate the formation of pore-blocking deposits. Due to the 50% relative humidity in a conditioned room, no additional crystalline deposits formed due to the lack of moisture. As a result, there is no difference in shrinkage reduction when comparing 7-day and 28-day shrinkage for the CA-cement composites. Overall, while promoting proper self-healing efficiency as mentioned by many studies (Zhang et al., 2021; Li et al., 2020a; Azarsa et al., 2019), the addition of CA slightly mitigates the total shrinkage of the cementitious composites. Meanwhile, by comparing the shrinkage reduction rate between CA and CA15 group, higher dosage of CA powder does not reduce the shrinkage deformation.

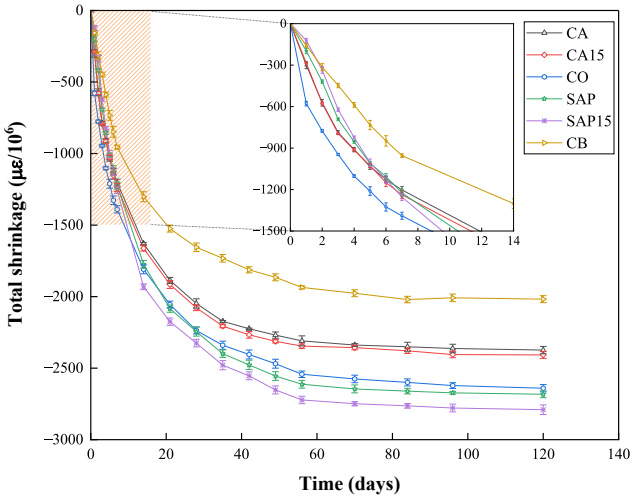

Fig. 7. Total shrinkage results.

Fig. 7 clearly depicts that SAP addition increases the long-term total shrinkage of the SP-cement composites when compared to SP-free control group. However, at an early age up to 7 days, the shrinkage results of SAP (green line) and SAP15 group (purple line) are reduced by 11% and 9.7% respectively. This is mainly due to the internal curing offered by SAP particles, releasing absorbed water to promote the hydration, being in good agreement with other studies (Wang et al., 2022a; Rostami et al., 2021). It should be noted that, the total shrinkage strains of the SAP-cementitious composites are higher than those of SAP-free samples starting from the second week of exposure. Several studies (Wang et al., 2016, 2022a) revealed that the primary reason was that most absorbed water was completely released after 7-day exposure, providing no further internal curing to mitigate the capillary pore forces after the second week. Likewise, Yang et al. (2019) pointed out that after releasing water, the decomposition of SAP gel created larger pores in the cementitious matrix, increasing the water evaporation rate. The evidence could be found in Fig. 7, where the shrinkage deformation of SAP and SAP15 group remained sharply during the second week of exposure. Furthermore, considering 120-day exposure, 2% and 5.7% increment of shrinkage strains is observed for SAP and SAP15 group when compared to the reference group. The higher shrinkage strains are related to higher water evaporation rate being consistent with other literature (Wang et al., 2022a; Yang et al., 2019). Wang et al. (2022a) suggested that higher dosage of SAP induced more pore defects, creating more channels for water to escape from the cementitious matrix.

By replacing cement with 2 wt% WWB, the total shrinkage strains of the WWB-cement composites are significantly reduced in Fig. 7. Similar to autogenous shrinkage, CB group (WWB and CA addition) shows favourable mitigation on the total shrinkage strains, being significantly lower than that of CA group (CA addition only). For 7-day curing, the total shrinkage deformations of CB group are reduced by 31.3% compared to that of CO group. As aforementioned, WWB gradually releases water to promote additional hydration, and refining porosity to reduce capillary pore tensions. Unlike decomposition of SAP particles after water releasing, WWB particles remains porous structure providing additional hydration sites, reducing potential the formation of pore defects. Likewise, Senadheera et al. (2023) pointed that the porous nature of biochar provided more hydration sites to densify the cementitious matrix, leading to a reduction of water evaporation. The evidence could be found in Fig. 8(a) and (b), showing that porous WWB particles provide more sites for cement hydration, as hydration products could be found in WWB pores and on WWB surface in Fig. 8(a) and (b).

Fig. 9 depicts the Ca/Si ratio comparison for hydration products at different locations by using EDS analysis. The highest average Ca/Si ratio (3.52) is found in location 3, while the lowest average Ca/Si ratio (1.71) is found in location 4. The common Ca/Si ratio of C–S–H gel from alite hydration is 1.7–1.8 (Cuesta et al., 2021), while lower Ca/Si ratio is 0.8–1.4 (Deschner et al., 2012; Wang et al., 2022b). Likewise, Guesta et al. (Cuesta et al., 2018) summarised that C–S–H gel with Ca/Si ratio of 1.67–2.5 was classified as inner C–S–H gel, and C–S–H gel with Ca/Si ratio higher than 2.5 indicted outer C–S–H gel. Aghaee and Khayat (2023) revealed that outer C–S–H gel was porous and bound with calcium hydroxide, being in a good agreement with several other studies (Chen et al., 2004; Kunther et al., 2017). As a result, the hydration products at location 2 and location 4 could be classified as C–S–H gel, while the hydration products at the other 3 locations could be the mix of C–S–H gel and calcium hydroxide. Based on several studies (Aghaee and Khayat, 2023; Babaahmadi et al., 2022), C–S–H gel with lower Ca/Si ratio demonstrated higher strength. As shown in Fig. 9, C–S–H gels at location 2, 4, and 5 would contribute to higher compressive strength than C–S–H gels at location 1 and 3, due to a denser morphology (Aghaee and Khayat, 2023). Nevertheless, WWB promotes a denser cementitious matrix by providing more hydration sites, leading to less water evaporation. Furthermore, finer-size WWB powder could act as

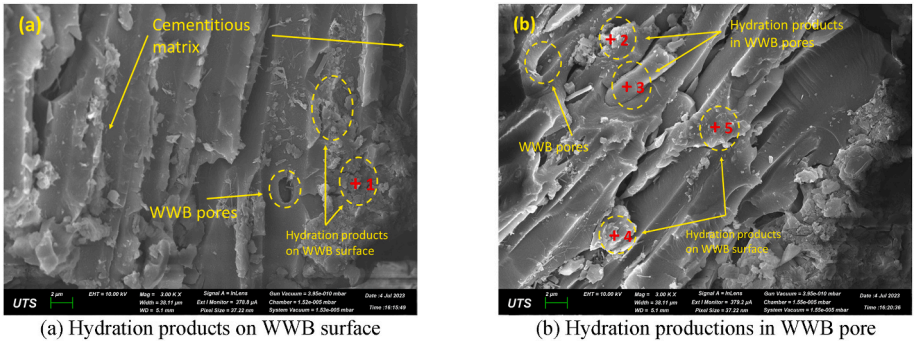

(a) Hydration products on WWB surface (b) Hydration productions in WWB pore

Fig. 8. Microstructures of CB group for total shrinkage experiment.

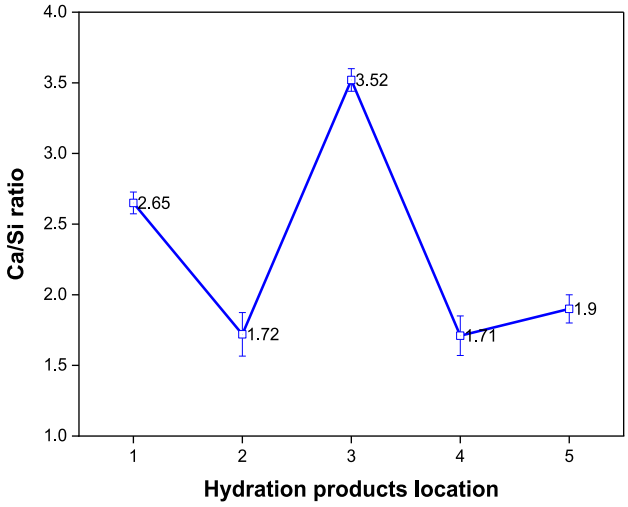

Fig. 9. Ca/Si ratio of hydration products at various locations.

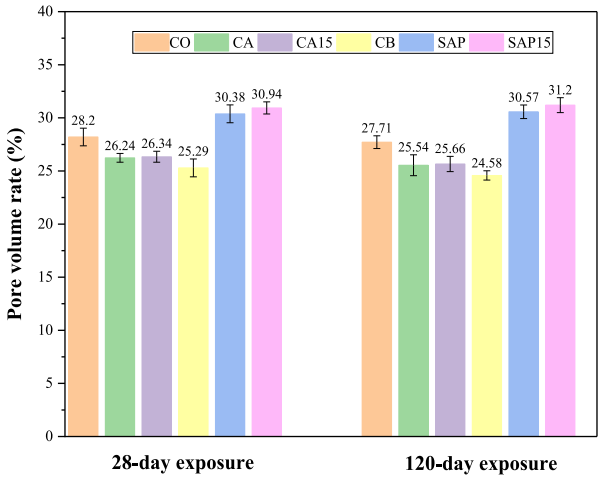

Fig. 10. Apparent porosity analysis at exposures of 28-day and 120-day.

fillers to block voids and pores, reducing the water evaporation rate. Similar findings could be found in existing literature (Lin et al., 2023; Gupta et al., 2020; Senadheera et al., 2023). For long-term curing, WWB addition promotes 26% and 23.6% reduction on the total shrinkage at 28-day and 120-day curing respectively. Similar to SAP particles, the water releasing process of WWB may stop at 7-day exposure, and the shrinkage reduction rate is decreasing accordingly. By considering these favourable benefits, the addition of WWB could significantly mitigate the total shrinkage of the biochar-cementitious composites.

3.3. Apparent porosity

The apparent porosity (AP) results at 28-day and 120-day are summarised in Fig. 10. When compared to the reference group, CA addition reduces AP by up to 7% at 28-day exposure. Considering the total shrinkage results provided in Fig. 7, the reduction of AP with CA addition is properly correlated with the lower total shrinkage strains of CA and CA15 group. In terms of CB group, the combination of CA and CB addition reduces AP by 10.3% at 28-day exposure. Since WWB addition promotes the cement hydration in Fig. 8(a) and (b) and fills in voids of the cementitious matrix, the highest reduction of AP is observed for this group. In correlation, the lowest total shrinkage results are observed for CB group in Fig. 7. Apparently, AP results at 120-day exposure, excepted for samples with SAP addition, decrease slightly when compared to that of 28-day exposure, having a good agreement with other studies (Ahmadi Moghadam et al., 2020; Mo et al., 2016). Based on the study by Qin et al. (2018), the compactness of the cementitious matrix was slightly increased with the increase of the exposure period in the air, resulting in a slight reduction in long-term apparent porosity.

However, the addition of SAP increases the 28-day AP by 7.3% and 9.7% for SAP and SAP 15 group respectively when compared to the reference CO group. Due to the decomposition of SAP after releasing absorbed moisture, additional pores were formed, leading to increased AP of SAP and SAP15 group. Further evidence could be found in Fig. 10, where slight increase in 120-day AP of samples with SAP addition is observed. In correlation with the total shrinkage strains in Fig. 7, unlike the mitigation of the autogenous shrinkage by SAP addition, the addition of SAP inevitably increases AP of the cementitious composites, leading to higher total shrinkage strains. Meanwhile, higher dosage of SAP further increases the total shrinkage strains and AP of the SAP-cementitious composites.

Overall, the apparent porosity results are highly correlated with the total shrinkage strains for all cementitious composites. Samples with lower AP have lower total shrinkage strains when compared to samples with higher AP. Although SAP addition completely mitigates the autogenous shrinkage, due to the decomposition of SAP particles, SAP addition increases the total shrinkage and leads to higher AP. The addition of CA presents an opposite trend, as CA addition has a negligible effect on the autogenous shrinkage, while slightly reducing both total shrinkage strain and AP. Moreover, CB group shows the best performances in reducing autogenous, total shrinkage strains and AP. The primary reason is that WWB addition further promotes the compactness of the biochar-cementitious composites.

3.4. Accelerated mortar bar test

Fig. 11 presents the average mortar expansion results up to 120-day exposure to the 1 M NaOH solution bath at 80 °C and each expansion point is the average of three identical samples. As recommended by AS1141.60.1 (AS 1141, 2014), the expansion limit of reactive aggregate at 10 days and 21 days is 0.1% and 0.3% respectively. It could be observed that the 10-day and 21-day mortar expansion of CO group is approximately 0.53% and 0.59% respectively in Fig. 11, confirming the high reactivity of dacite sand against the expansion limit as suggested by AS1141.60.1 (AS 1141, 2014). According to Fig. 11, the reference CO group (blue line) has the highest level of mortar expansion, which is expected, since there is no mitigation strategy against the alkali-silica reaction. It could be observed that there is a high reactivity of the reference CO group at early age, as the 7-day expansion is 0.52%. The expansion rate of CO group is gradually reduced over time, being consistent with other studies (Ma et al., 2023; Nguyen et al., 2020). For the long-term NaOH solution exposure, 0.62% and 0.8% mortar expansion are observed at 28-day and 120-day respectively.

CA addition leads to significant reduction in the mortar expansions in Fig. 11. At 7-day exposure, the average mortar expansion is approximately 0.14% (black line), significantly reducing the expansion by 72.4% when compared to that of the refence group (blue line). By adding 1 wt% PENETRON CA, it is observed that the 14-day and 28-day mortar expansions are reduced by 63.6% and 57.7% respectively. Similar finding is reported in the study with 1 wt% CA addition (Munhoz et al., 2021). Munhoz et al. (2021) reported that 1 wt% CA addition led to 75.4% and 64.5% expansion reduction at 14-day and 28-day exposure respectively. Jalali and Afgan (2018) explain that while promoting a denser cementitious matrix, CA addition denied the alkali ion penetrations mitigating the ASR expansions. Likewise, Liu (2011) reported that the addition of Xypex CA reduced the penetration depth of sodium ions, promoting the resistance against ASR expansions in the CA-cement composites.

The expansion reduction rates observed in this study are smaller than those reported by Munhoz et al. (2021). It should be noted that the different performance of the CA and the different level of reactivity contributed to the differences in ASR expansion observed in this study and in the experiment by Munhoz et al. (2021). However, a 57.7% reduction in 28-day mortar expansion could still be considered as an effective mitigation on the ASR expansion for the cementitious composites. After 120 days of 1 M NaOH solution exposure at 80 °C, the average expansion of CA group is 0.39%, reducing the expansion by 50.6%. It could be found that there is a decreasing trend on the ASR expansion reduction rate, reducing from 72.3% at 7-day to 50.6% at 120-day exposure. Although CA promotes a denser cementitious matrix, the continuous immersion in the 1 M NaOH solution at 80 °C allows more alkali ions reacting with reactive fine aggregates, creating more pores for sodium-ion penetration. Similarly, according to Munhoz et al. (2021), more ASR products were found at later immersing ages, due to sodium-ion penetration. As a result, CA promotes a smaller expansion reduction in 120-day testing time.

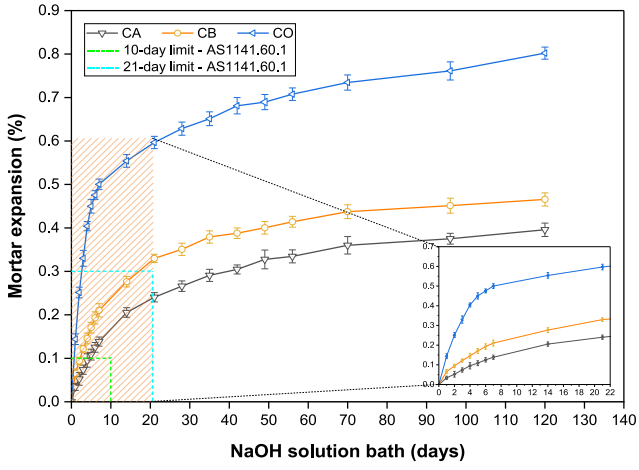

Fig. 11. ASR expansion comparison of self-healing biochar-cementitious composites.

Considering the effect of 2 wt% WWB, Fig. 11 indicates that the average expansion results of CB group (orange line) are significantly lower than that of the reference group. The mortar expansion is 0.21% and 0.35% at 7-day and 28-day exposure respectively, leading to a 57.9% and 44.2% reduction in expansion rate respectively. However, it should be noted that additional WWB particles leads to more expansion when compared to samples with CA addition only. Based on the XRF results in Table 1, SiO_2 of WWB is 58.20%, being higher than that of CA (14.15%) and cement (18.94%). Several studies (Lin et al., 2023; Nguyen, 2021) mentioned that the high content of amorphous silica exposed on the biochar surface was a favourable fact for the formation of C–S–H gel during hydration process. However, due to the porous nature of WWB, WWB with high silica content would act similarly to reactive sand, leading to additional ASR products. As a result, higher content of silica of WWB negatively affect the ASR mitigation in the biochar-cement composites. At 120-day curing, the average CB mortar expansion is 0.46%, being 42.9% less than that of CO group. It could be observed that similar to the trend of expansion reduction rate of CA group, there is also a decreasing trend in the expansion reduction rate due to WWB addition during the immersing age.

3.5. Microstructural analysis

Fig. 12 shows the SEM images of the ITZ of the different samples immersed for 28-day, at various magnifications, including CO group in Fig. 12(a) and (b), CA group in Fig. 12(c) and (d), and CB group in Fig. 12(e) and (f). In this study, due to the high reactivity of the fine aggregate, there is relatively higher formation of ASR gel at 28-day exposure, resulting to larger mortar expansions of the reference group in Fig. 11. The evidence could be found in Fig. 12(b). Apparent crack is observed between reactive aggregate and the cementitious matrix, reflecting the high alkali-silica reaction of CO group. Similar findings were reported by Joo et al. (Joo and Takahashi, 2023), confirming that due to the alkali attack, the excessive formations of ASR gel created cracks in the ITZ between reactive aggregates and the cementitious matrix.

According to Fig. 12(d), there are no apparent cracks within the ITZ of CA group, indicating less formations of ASR gels between reactive sand and the cementitious matrix. Gong et al. (2020) explained that due to continuous sodium attack, ASR products would deteriorate the stable ITZ between reactive aggregates and the cementitious matrix, leading to higher sample expansions. In this study, CA addition promotes a denser CA-cementitious matrix, significantly reducing the alkali access, mitigating the mortar expansion in Fig. 11. The reduced formation of ASR gels in the ITZ is highly related to the lower mortar expansions, verifying that CA addition could improve the resistance against the alkali-silica reaction. Fig. 12(f) depicts the ITZ of CB group, and less cracks are observed within the ITZ when compared to that of CO group in Fig. 12 (b). The combination of CA and WWB addition reduces the penetration depth of sodium ions, leading to less mortar expansions during the immersion period. However, the presence of WWB provides additional source of amorphous silica, leading to higher mortar expansions, compared to mortars containing on CA.

By combining Figs. 11 and 12, a high correlation between the mortar expansions and the cracks formation within the ITZ of samples is observed. For CO group, it is observed that the excessive formations of ASR products lead to more cracks in the ITZ in Fig. 12(b), leading to the highest mortar expansions. Since CA promotes a denser cementitious

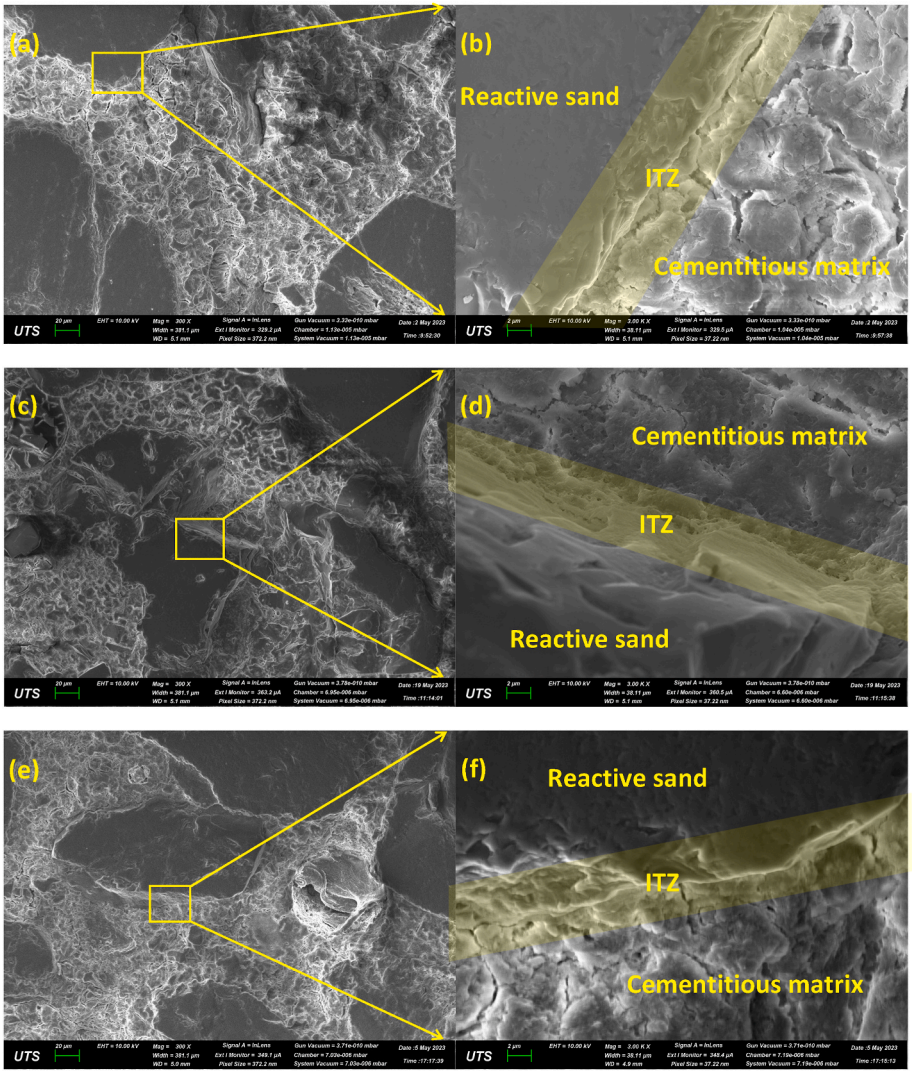

Fig. 12. Microstructures of ITZs in different samples: (a) CO group; (b) ITZ amplification in CO group; (c) CA group; (d) ITZ amplification in CA group; (e) CB group; (f) ITZ amplification in CB group.

matrix, less ASR products and cracks are found in the ITZ of CA samples. Meanwhile, CA samples shows the lowest mortar expansions. However, due to the high silica content in WWB, the porous WWB microstructure allows more ASR products formation by consuming amorphous silica in WWB. As a result, several cracks are observed in the ITZ of CB group, and the mortar expansion of CB group is higher than that of CA group.

4. Conclusions

This study investigated the effects of CA addition on shrinkage and alkali-silica reaction of the cementitious composites with and without WWB. Some conclusions could be summarised as the follows.

(1) The 1–1.5 wt% CA addition has no effect on the mitigation of autogenous shrinkage of the cementitious composites. 1–1.5 wt% SAP addition could completely mitigate the autogenous shrinkage of the cementitious matrix. The combination of 1 wt% CA and 2 wt% WWB promotes a proper reduction (24.23% reduction) in the autogenous shrinkage of CB group at 120 days.
(2) By promoting a denser cementitious matrix to prevent water moisture evaporation, 1.0 wt% CA addition leads to 10.1% total shrinkage reduction, and 1.5 wt% CA reduces the total shrinkage by 9.2% at 120-day exposure.
(3) Due to the decomposition of SAP particles after releasing water, more pores and voids formed increasing the water evaporation rate, slightly increasing the total shrinkage (2% and 5.7% increment for 1 wt% and 1.5 wt% SAP addition respectively). Higher dosage of SAP addition further increases the total shrinkage.
(4) For CB group, fine WWB particle fills the voids and pores leading to a denser cementitious microstructure, and porous WWB provides more sites for hydration. Additionally, C–S–H gel forms in the pores of WWB and on the surface of WWB. As a result, WWB leads to 23.6% reduction on 120-day total shrinkage.
(5) The results of apparent porosity are highly correlated with the results of total shrinkage for all cementitious samples. 1–1.5 wt% SAP addition increases the total shrinkage of the cementitious composites with the highest apparent porosity, while 1–1.5 wt% CA addition slightly reduces the total shrinkage of the CA-cement composites and leads to a lower apparent porosity. CB samples were measured the lowest total shrinkage and the lowest apparent porosity.
(6) Due to excessive formations of ASR products, CO group showed the highest mortar expansion. 1 wt% CA addition could significantly reduce the alkali attack, significantly mitigating the mortar expansions with less formation of ASR products in the ITZ.

However, the additional WWB addition led to a higher mortar expansion.

(7) Current results suggests that CA addition could also lead to lower shrinkage and ASR expansion of the CA-cement composites, suggesting that it could be conservatively used as self-healing agent in Australia. The addition of WWB promotes the resistance of shrinkage deformation and ASR expansion for biochar-cement composites, indicating that it is feasible to recycle waste wood in Australia to produce waste wood biochar.

(8) Although systematic analysis is carried out to investigate the influence of CA on the shrinkage and alkali-silica reaction of the cementitious composites, more studies are needed for a more comprehensive conclusion on the actual effects of CA addition. Particularly, accelerated mortar bar test (AMBT) could only provide preliminary results for the ASR analysis, being used as reference results.

CRediT authorship contribution statement

Xuqun Lin: Writing – review & editing, Writing – original draft, Methodology, Investigation, Formal analysis, Data curation. **Arnaud Castel:** Writing – review & editing, Writing – original draft, Validation, Funding acquisition. **Zhizhong Deng:** Writing – review & editing, Writing – original draft. **Biqin Dong:** Writing – review & editing, Writing – original draft. **Xuanrui Zhang:** Writing – review & editing, Writing – original draft. **Shishun Zhang:** Writing – review & editing, Validation. **Wengui Li:** Writing – review & editing, Writing – original draft, Validation, Funding acquisition, Conceptualization.

Declaration of competing interest

The authors declare that they have no known competing financial interests or personal relationships that could have appeared to influence the work reported in this paper.

Data availability

Data will be made available on request.

Acknowledgements

The authors would like to appreciate Australian Research Council (DP220101051; DP220100036), Australia and University of Technology Sydney Research Academic Program at Tech Lab (UTS RAPT) for the kind supports.

Appendix A. Supplementary data

Supplementary data to this article can be found online at https://doi.org/10.1016/j.dibe.2024.100456.

References

Aghaee, K., Khayat, K.H., 2022. Benefits and drawbacks of using multiple shrinkage mitigating strategies on performance of fiber-reinforced mortar. Cement Concr. Compos. 133, 104714.

Aghaee, K., Khayat, K.H., 2023. Effect of internal curing and shrinkage-mitigating materials on microstructural characteristics of fiber-reinforced mortar. Construct. Build. Mater. 386, 131527.

Aghaee, K., Sposito, R., Thienel, K.-C., Khayat, K.H., 2023. Effect of additional water or superplasticizer on key characteristics of cement paste made with superabsorbent polymer and other shrinkage mitigating materials. Cement Concr. Compos. 136, 104893.

Ahmadi Moghadam, H., Mirzaei, A., Abedi Dehghi, Z., 2020. The relation between porosity, hydration degree and compressive strength of Portland cement pastes in the presence of aluminum chloride additive. Construct. Build. Mater. 250, 118884.

Akhtar, M.K., Kanwal, M., Khushnood, R.A., Khan, M.B.E., 2023. Assessment of mechanical attributes and microstructural densification of self-healing recycled coarse aggregate concrete using various bacterial immobilizers. J. Build. Eng. 69, 106229.

Amjad, H., Arsalan Khushnood, R., Ali Memon, S., 2023. Biomimetic robust self-healing of Bacillus Subtilis immobilized through sisal fiber for next-generation concrete infrastructure. Construct. Build. Mater. 368, 130299.

AS 1141, 2014. 60.1 Methods for Sampling and Testing Aggregates Method 60.1: Potential Alkali-Silica Reactivity-Accelerated Mortar Bar Method. Standard Australia, Sydney, Australia.

AS 2350, 2006. 13 Methods of Testing Portland, Blended and Masonry Cements, Method 13: Determination of Drying Shrinkage of Cement Mortars. Standard Australia, Sydney, Australia.

Azarsa, P., Gupta, R., Biparva, A., 2019. Assessment of self-healing and durability parameters of concretes incorporating crystalline admixtures and Portland Limestone Cement. Cement Concr. Compos. 99, 17–31.

Babaahmadi, A., Machner, A., Kunther, W., Figueira, J., Hemstad, P., De Weerdt, K., 2022. Chloride binding in Portland composite cements containing metakaolin and silica fume. Cement Concr. Res. 161, 106924.

Borg, R.P., Cuenca, E., Gastaldo Brac, E.M., Ferrara, L., 2018. Crack sealing capacity in chloride-rich environments of mortars containing different cement substitutes and crystalline admixtures. J. Sustain. Cement-Based Mater. 7 (3), 141–159.

Cappellesso, V.G., Van Mullem, T., Gruyaert, E., Van Tittelboom, K., De Belie, N., 2023a. Bacteria-based self-healing concrete exposed to frost salt scaling. Cement Concr. Compos. 139, 105016.

Cappellesso, V., di Summa, D., Pourhaji, P., Prabhu Kannikachalam, N., Dabral, K., Ferrara, L., Cruz Alonso, M., Camacho, E., Gruyaert, E., De Belie, N., 2023b. A review of the efficiency of self-healing concrete technologies for durable and sustainable concrete under realistic conditions. Int. Mater. Rev. 68 (5), 556–603.

Cassidy, M., Waldie, J., Palanisamy, S., 2015. A method to estimate the cost of corrosion for Australian defence force aircraft. In: Proc., 16th Australian Int. Aerospace Congress. Melbourne, Australia. Barton. ACT, Australia: Engineers Australia.

Chandra, T.S.R., Ravitheja, A., 2019. Macro mechanical properties of self healing concrete with crystalline admixture under different environments. Ain Shams Eng. J. 10 (1), 23–32.

Chen, J.J., Thomas, J.J., Taylor, H.F.W., Jennings, H.M., 2004. Solubility and structure of calcium silicate hydrate. Cement Concr. Res. 34 (9), 1499–1519.

Chindasiriphan, P., Yokota, H., Pimpakan, P., 2020. Effect of fly ash and superabsorbent polymer on concrete self-healing ability. Construct. Build. Mater. 233, 116975.

Cuenca, E., Mezzena, A., Ferrara, L., 2021. Synergy between crystalline admixtures and nano-constituents in enhancing autogenous healing capacity of cementitious composites under cracking and healing cycles in aggressive waters. Construct. Build. Mater. 266, 121447.

Cuesta, A., Zea-Garcia, J.D., Londono-Zuluaga, D., De la Torre, A.G., Santacruz, I., Vallcorba, O., Dapiaggi, M., Sanfélix, S.G., Aranda, M.A., 2018. Multiscale understanding of tricalcium silicate hydration reactions. Sci. Rep. 8 (1), 8544.

Cuesta, A., Santacruz, I., De la Torre, A.G., Dapiaggi, M., Zea-Garcia, J.D., Aranda, M.A. G., 2021. Local structure and Ca/Si ratio in C-S-H gels from hydration of blends of tricalcium silicate and silica fume. Cement Concr. Res. 143, 106405.

De Meyst, L., Mannekens, E., Van Tittelboom, K., De Belie, N., 2021. The influence of superabsorbent polymers (SAPs) on autogenous shrinkage in cement paste, mortar and concrete. Construct. Build. Mater. 286, 122948.

De Nardi, C., Gardner, D., Cristofori, D., Ronchin, L., Vavasori, A., Jefferson, T., 2023. Advanced 3D printed mini-vascular network for self-healing concrete. Mater. Des. 230, 111939.

De Souza, D.J., Sanchez, L.F.M., 2023. Understanding the efficiency of autogenous and autonomous self-healing of conventional concrete mixtures through mechanical and microscopical analysis. Cement Concr. Res. 172, 107219.

de Souza Oliveira, A., da Fonseca Martins Gomes, O., Ferrara, L., de Moraes Rego Fairbairn, E., Toledo Filho, R.D., 2021. An overview of a twofold effect of crystalline admixtures in cement-based materials: from permeability-reducers to self-healing stimulators. J. Build. Eng. 41, 102400.

Deschner, F., Winnefeld, F., Lothenbach, B., Seufert, S., Schwesig, P., Dittrich, S., Goetz-Neunhoeffer, F., Neubauer, J., 2012. Hydration of Portland cement with high replacement by siliceous fly ash. Cement Concr. Res. 42 (10), 1389–1400.

Dong, W., Li, W., Shen, L., Zhang, S., Vessalas, K., 2021. Integrated self-sensing and self-healing cementitious composite with microencapsulation of nano-carbon black and slaked lime. Mater. Lett. 282, 128834.

Dong, W., Li, W., Wang, K., Shah, S.P., Sheng, D., 2022. Multifunctional cementitious composites with integrated self-sensing and self-healing capacities using carbon black and slaked lime. Ceram. Int. 48 (14), 19851–19863.

FloresM, R., Moscato, S., Serna, P., Ferrara, L., 2015. Self-healing capability of concrete with crystalline admixtures in different environments. Construct. Build. Mater. 86, 1–11.

Gong, F., Takahashi, Y., Segawa, I., Maekawa, K., 2020. Mechanical properties of concrete with smeared cracking by alkali-silica reaction and freeze-thaw cycles. Cement Concr. Compos. 111, 103623.

Guan, X., Zhang, C., Li, Y., Zhao, S., 2020. Effect of exposure conditions on self-healing behavior of engineered cementitious composite incorporating limestone powder. Cement Concr. Compos. 114, 103808.

Guizani, C., Jeguirim, M., Valin, S., Limousy, L., Salvador, S., 2017. Biomass chars: the effects of pyrolysis conditions on their morphology, structure, chemical properties and reactivity. Energies 10 (6), 796.

Gupta, S., Kua, H.W., 2018. Effect of water entrainment by pre-soaked biochar particles on strength and permeability of cement mortar. Construct. Build. Mater. 159, 107–125.

Gupta, S., Kua, H.W., 2019. Carbonaceous micro-filler for cement: effect of particle size and dosage of biochar on fresh and hardened properties of cement mortar. Sci. Total Environ. 662, 952–962.

Gupta, S., Kua, H.W., Pang, S.D., 2018. Biochar-mortar composite: manufacturing, evaluation of physical properties and economic viability. Construct. Build. Mater. 167, 874–889.
Gupta, S., Krishnan, P., Kashani, A., Kua, H.W., 2020. Application of biochar from coconut and wood waste to reduce shrinkage and improve physical properties of silica fume-cement mortar. Construct. Build. Mater. 262, 120688.
Hermawan, H., Wiktor, V., Gruyaert, E., Serna, P., 2023. Experimental investigation on the bond behaviour of steel reinforcement in self-healing concrete. Construct. Build. Mater. 383, 131378.
Hu, X., Xiao, J., Zhang, Z., Wang, C., Long, C., Dai, L., 2022. Effects of CCCW on properties of cement-based materials: a review. J. Build. Eng. 50, 104184.
Jalali, U.H., Afgan, S., 2018. Analysis of integral crystalline waterproofing technology for concrete. Int. Res. J. Eng. Technol. (IRJET) 5 (10), 1076–1085.
Javed, M.H., Ali Sikandar, M., Ahmad, W., Tariq Bashir, M., Alrowais, R., Bilal Wadud, M., 2022. Effect of various biochars on physical, mechanical, and microstructural characteristics of cement pastes and mortars. J. Build. Eng. 57, 104850.
Joo, H.E., Takahashi, Y., 2023. Analytical and experimental studies on alkali-silica reaction mechanism: aggregate cracking and chemical composition change of gel. Cement Concr. Compos. 139, 105003.
Kua, H.W., Tan, S.M.H., 2023. Novel typology of accelerated carbonation curing: using dry and pre-soaked biochar to tune carbon capture and mechanical properties of cementitious mortar. Biochar 5 (1), 36.
Kunther, W., Ferreiro, S., Skibsted, J., 2017. Influence of the Ca/Si ratio on the compressive strength of cementitious calcium–silicate–hydrate binders. J. Mater. Chem. A 5 (33), 17401–17412.
Lauch, K.S., Charron, J.P., Desmettre, C., 2022a. Comprehensive evaluation of self-healing of concrete with different admixtures under laboratory and long-term outdoor expositions. J. Build. Eng. 54, 104661.
Lauch, K.S., Desmettre, C., Charron, J.P., 2022b. Self-healing of concrete containing different admixtures under laboratory and long-term real outdoor expositions based on water permeability test. Construct. Build. Mater. 324, 126700.
Li, G., Liu, S., Niu, M., Liu, Q., Yang, X., Deng, M., 2020a. Effect of granulated blast furnace slag on the self-healing capability of mortar incorporating crystalline admixture. Construct. Build. Mater. 239, 117818.
Li, Z., Wyrzykowski, M., Dong, H., Granja, J., Azenha, M., Lura, P., Ye, G., 2020b. Internal curing by superabsorbent polymers in alkali-activated slag. Cement Concr. Res. 135, 106123.
Lin, X., Li, W., Guo, Y., Dong, W., Castel, A., Wang, K., 2023. Biochar-cement concrete toward decarbonisation and sustainability for construction: characteristic, performance and perspective. J. Clean. Prod., 138219
Liu, T., 2011. Analysis of Performance and Function of Composition of Cementitious Capillary Crystalline Waterproof Materials. Tsinghua University, Beijing, China.
Liu, C., Zhang, R., Liu, H., Nong, X., 2022. Self-healing concrete with recycled coarse aggregate: the performance of biochemical-chloride ion transport. J. Build. Eng. 57, 104925.
Lucas, S.S., von Tapavicza, M., Schmidt, A.M., Bertling, J., Nellesen, A., 2016. Study of quantification methods in self-healing ceramics, polymers and concrete: a route towards standardization. J. Intell. Mater. Syst. Struct. 27 (19), 2577–2598.
Ma, P., Li, J., Bai, J., Zhuo, Y., Chi, L., Zhu, Y., Shi, Z., Ma, H., Chen, G., 2023. Effect of type and quantity of inherent alkali cations on alkali-silica reaction. Cement Concr. Res. 173, 107293.
Macdonald, D.D., Zhu, Y., Yang, J., Qiu, J., Engelhardt, G.R., Sagüés, A., Sun, L., Xiong, Z., 2021. Corrosion of rebar in concrete. Part IV. On the theoretical basis of the chloride threshold. Corrosion Sci. 185, 109460.
Mo, L., Zhang, F., Deng, M., 2016. Mechanical performance and microstructure of the calcium carbonate binders produced by carbonating steel slag paste under CO2 curing. Cement Concr. Res. 88, 217–226.
Mo, L., Fang, J., Huang, B., Wang, A., Deng, M., 2019. Combined effects of biochar and MgO expansive additive on the autogenous shrinkage, internal relative humidity and compressive strength of cement pastes. Construct. Build. Mater. 229, 116877.
Moelich, G.M., Kruger, P.J., Combrinck, R., 2022. Mitigating early age cracking in 3D printed concrete using fibres, superabsorbent polymers, shrinkage reducing admixtures, B-CSA cement and curing measures. Cement Concr. Res. 159, 106862.
Mohammed, A.A., Manalo, A.C., Maranan, G.B., Muttashar, M., Zhuge, Y., Vijay, P.V., Pettigrew, J., 2020. Effectiveness of a novel composite jacket in repairing damaged reinforced concrete structures subject to flexural loads. Compos. Struct. 233, 111634.
Munhoz, G.S., Dobrovolski, M.E.G., Pereira, E., Medeiros-Junior, R.A., 2021. Effect of improved autogenous mortar self-healing in the alkali-aggregate reaction. Cement Concr. Compos. 117, 103905.
Munn, R.L., Kao, G., Chang, Z.-T., 2003. Performance and compatibility of permeability reducing and other chemical admixtures in Australian concretes. In: Proceedings of 7th CANMET/ACI Int. Conference on Superplasticizers and Other Chemical Admixtures in Concrete, pp. 361–379.
Nguyen, M.N., 2021. Potential use of silica-rich biochar for the formulation of adaptively controlled release fertilizers: a mini review. J. Clean. Prod. 307, 127188.
Nguyen, Q.D., Kim, T., Castel, A., 2020. Mitigation of alkali-silica reaction by limestone calcined clay cement (LC3). Cement Concr. Res. 137, 106176.
Penetron, 2023. Penetron Admix safety data sheet. https://www.penetron.com/products/PENETRON-ADMIX/safety-data-sheet.pdf.
Qin, L., Gao, X., Li, Q., 2018. Upcycling carbon dioxide to improve mechanical strength of Portland cement. J. Clean. Prod. 196, 726–738.
Rostami, R., Klemm, A.J., Almeida, F.C.R., 2021. Reduction of shrinkage by Superabsorbent polymers (SAP) in fibre reinforced mortars. Construct. Build. Mater. 288, 123109.
Senadheera, S.S., Gupta, S., Kua, H.W., Hou, D., Kim, S., Tsang, D.C.W., Ok, Y.S., 2023. Application of biochar in concrete – a review. Cement Concr. Compos. 143, 105204.
Sisomphon, K., Copuroglu, O., Koenders, E.A.B., 2013. Effect of exposure conditions on self healing behavior of strain hardening cementitious composites incorporating various cementitious materials. Construct. Build. Mater. 42, 217–224.
Snoeck, D., Jensen, O.M., De Belie, N., 2015. The influence of superabsorbent polymers on the autogenous shrinkage properties of cement pastes with supplementary cementitious materials. Cement Concr. Res. 74, 59–67.
Su, Y., Qian, C., Rui, Y., Feng, J., 2021. Exploring the coupled mechanism of fibers and bacteria on self-healing concrete from bacterial extracellular polymeric substances (EPS). Cement Concr. Compos. 116, 103896.
Tian, Y., Bao, J., Guo, W., Zhang, P., Cui, Y., Zhao, T., 2022. Autogenous self-healing of cracked concrete exposed to the marine tidal zone. Construct. Build. Mater. 357, 129336.
Tu, W., Zhu, Y., Fang, G., Wang, X., Zhang, M., 2019. Internal curing of alkali-activated fly ash-slag pastes using superabsorbent polymer. Cement Concr. Res. 116, 179–190.
Van Tittelboom, K., De Belie, N., 2013. Self-healing in cementitious materials—a review. Materials 6 (6), 2182–2217.
Wan, Z., Zhang, Y., Xu, Y., Šavija, B., 2023a. Self-healing cementitious composites with a hollow vascular network created using 3D-printed sacrificial templates. Eng. Struct. 289, 116282.
Wan, Z., Chang, Z., Xu, Y., Šavija, B., 2023b. Optimization of vascular structure of self-healing concrete using deep neural network (DNN). Construct. Build. Mater. 364, 129955.
Wang, F., Yang, J., Hu, S., Li, X., Cheng, H., 2016. Influence of superabsorbent polymers on the surrounding cement paste. Cement Concr. Res. 81, 112–121.
Wang, L., Zhang, G., Wang, P., Yu, S., 2018. Effects of fly ash and crystalline additive on mechanical properties of two-graded roller compacted concrete in a high RCC arch dam. Construct. Build. Mater. 182, 682–690.
Wang, J., Xu, H., Xu, D., Du, P., Zhou, Z., Yuan, L., Cheng, X., 2019a. Accelerated carbonation of hardened cement pastes: influence of porosity. Construct. Build. Mater. 225, 159–169.
Wang, J.-Y., Chen, Z.-Z., Wu, K., 2019b. Properties of calcium sulfoaluminate cement made ultra-high performance concrete: tensile performance, acoustic emission monitoring of damage evolution and microstructure. Construct. Build. Mater. 208, 767–779.
Wang, X., Chen, S., Ren, J., Huang, R., Yang, Z., Wang, W., Liu, J., 2022a. Effect of super absorbent polymer and mineral additives on mechanical, shrinkage and healing properties of self-healing lightweight aggregate concrete under different curing regimes. Construct. Build. Mater. 357, 129377.
Wang, J., Hu, Z., Chen, Y., Huang, J., Ma, Y., Zhu, W., Liu, J., 2022b. Effect of Ca/Si and Al/Si on micromechanical properties of C(-A)-S-H. Cement Concr. Res. 157, 106811.
Wang, R., Ding, Z., Zhang, Y., Xu, Y., 2023. Self-healing of high-performance engineered cementitious materials with crystalline admixture in the seawater environment. J. Build. Eng. 63, 105472.
Wongkeo, W., Thongsanitgarn, P., Chaipanich, A., 2012. Compressive strength and drying shrinkage of fly ash-bottom ash-silica fume multi-blended cement mortars. Mater. Des. 36, 655–662, 1980-2015.
Wu, M., Hu, X., Zhang, Q., Cheng, W., Xue, D., Zhao, Y., 2020. Application of bacterial spores coated by a green inorganic cementitious material for the self-healing of concrete cracks. Cement Concr. Compos. 113, 103718.
Xiao, X., Unluer, C., Chu, S., Yang, E.-H., 2023. Single bacteria spore encapsulation through layer-by-layer self-assembly of poly(dimethyldiallyl ammonium chloride) and silica nanoparticles for self-healing concrete. Cement Concr. Compos. 140, 105105.
Xue, C., Li, W., Qu, F., Sun, Z., Shah, S.P., 2020. Self-healing efficiency and crack closure of smart cementitious composite with crystalline admixture and structural polyurethane. Construct. Build. Mater. 260, 119955.
Xu, Y., Wang, X.Y., 2021. Strength and durability improvements of biochar-blended mortar or paste using accelerated carbonation curing. J. CO2 Util. 54, 101766.
Xue, C., Li, W., Li, J., Wang, K., 2019. Numerical investigation on interface crack initiation and propagation behaviour of self-healing cementitious materials. Cem. Concr. Res. 122, 1–16.
Xue, C., Li, W., Luo, Z., Wang, K., Castel, A., 2021. Effect of chloride ingress on self-healing recovery of smart cementitious composite incorporating crystalline admixture and MgO expansive agent. Cement Concr. Res. 139, 106252.
Xue, C., Li, W., Wang, K., Sheng, D., Shah, S.P., 2020. Novel experimental and numerical investigations on bonding behaviour of crack interface in smart self-healing concrete. Smart Mater. Struct. 29, 085004.
Yang, J., Liu, L., Liao, Q., Wu, J., Li, J., Zhang, L., 2019. Effect of superabsorbent polymers on the drying and autogenous shrinkage properties of self-leveling mortar. Construct. Build. Mater. 201, 401–407.
Zeinali, F., Ahmadi, J., Rahmani, H., 2023. Self–healing capacity assessment of cracked slag modified concrete under different re-curing conditions. Construct. Build. Mater. 385, 131512.
Zhang, C., Lu, R., Li, Y., Guan, X., 2021. Effect of crystalline admixtures on mechanical, self-healing and transport properties of engineered cementitious composite. Cement Concr. Compos. 124, 104256.
Zheng, K., Yang, X., Chen, R., Xu, L., 2019. Application of a capillary crystalline material to enhance cement grout for sealing tunnel leakage. Construct. Build. Mater. 214, 497–505.